jitc-2020-001846.R2

## Supplemental Information

# Δ133p53α enhances metabolic and cellular fitness of TCR-engineered T cells and promotes superior antitumor immunity

**Authors:** Kevin J. Legscha[1], Edite A. Ferreira[1], Antonios Chamoun[1], Alexander Lang[1], Mohamed HS. Awwad[2], Gigi NHQ Ton[2], Danuta Galetzka[3], Borhane Guezguez[1,4,5], Michael Hundemer[2], Jean-Christophe Bourdon[6], Markus Munder[1,7], Matthias Theobald[1,4,7], Hakim Echchannaoui[1,4]

**Affiliations:** [1]Third Department of Medicine, University Cancer Center (UCT), University Medical Center (UMC) of the Johannes Gutenberg University
[2]Department of Internal Medicine V, University of Heidelberg
[3]Department of Radiation Oncology and Radiotherapy, UMC of the Johannes Gutenberg University
[4]German Cancer Consortium (DKTK), Partner Site Frankfurt/Mainz, Mainz, Germany
[5]German Cancer Research Center (DKFZ), Heidelberg, Germany
[6]School of Medicine, University of Dundee, Dundee, UK
[7]Research Center for Immunotherapy, UMC of the Johannes Gutenberg University Mainz, Germany

**Correspondence to:** Hakim Echchannaoui | Tel: +49 6131 17-9722 | Email: echchann@uni-mainz.de

jitc-2020-001846.R2

## Supplemental data

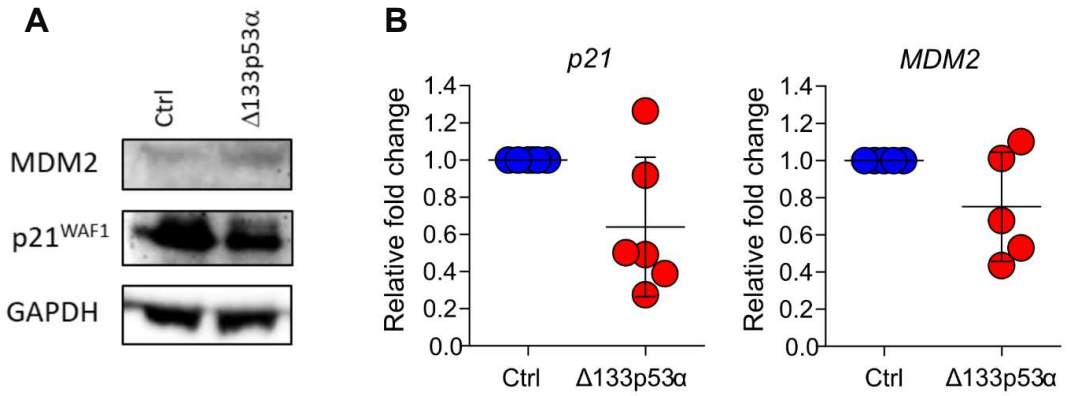


**Figure S1.** Δ133p53α modulates the function of the full-length p53. (A) Immunoblot analysis of the expression of $p21^{Waf1/Cip1}$ and MDM2 as p53 target genes in human $CD8^+$ T cells transduced with an empty control (ctrl) vector or retroviral vector encoding for Δ133p53α isoform. (B) Summary data from 5-6 heathy are shown. Data were normalized to GAPDH and shown as relative fold change to Ctrl samples.

jitc-2020-001846.R2

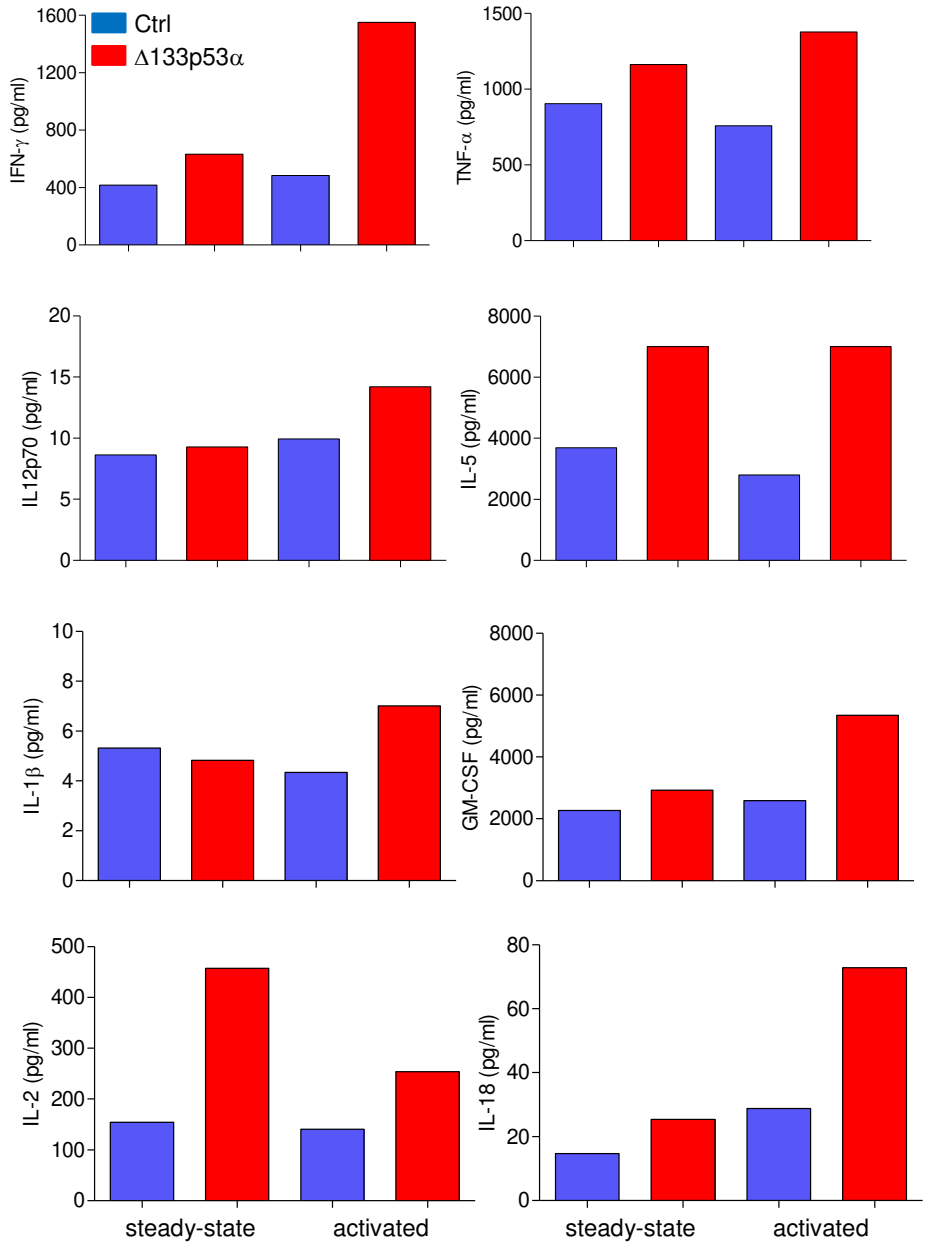


**Figure S2.** Δ133p53α invigorates cytokine response of antigen TCR-engineered T cells. Cytokine profiles of Δ133p53α-overexpressing and control T cells under steady-state (=resting) and after tumor antigen encounter (=activated) as measured by Multiplex Immunoassay at late stage in vitro culture. For activation, T cells were cultured over 24 hours with target tumor cells Saos2/143 (E:T = 1:1).

jitc-2020-001846.R2

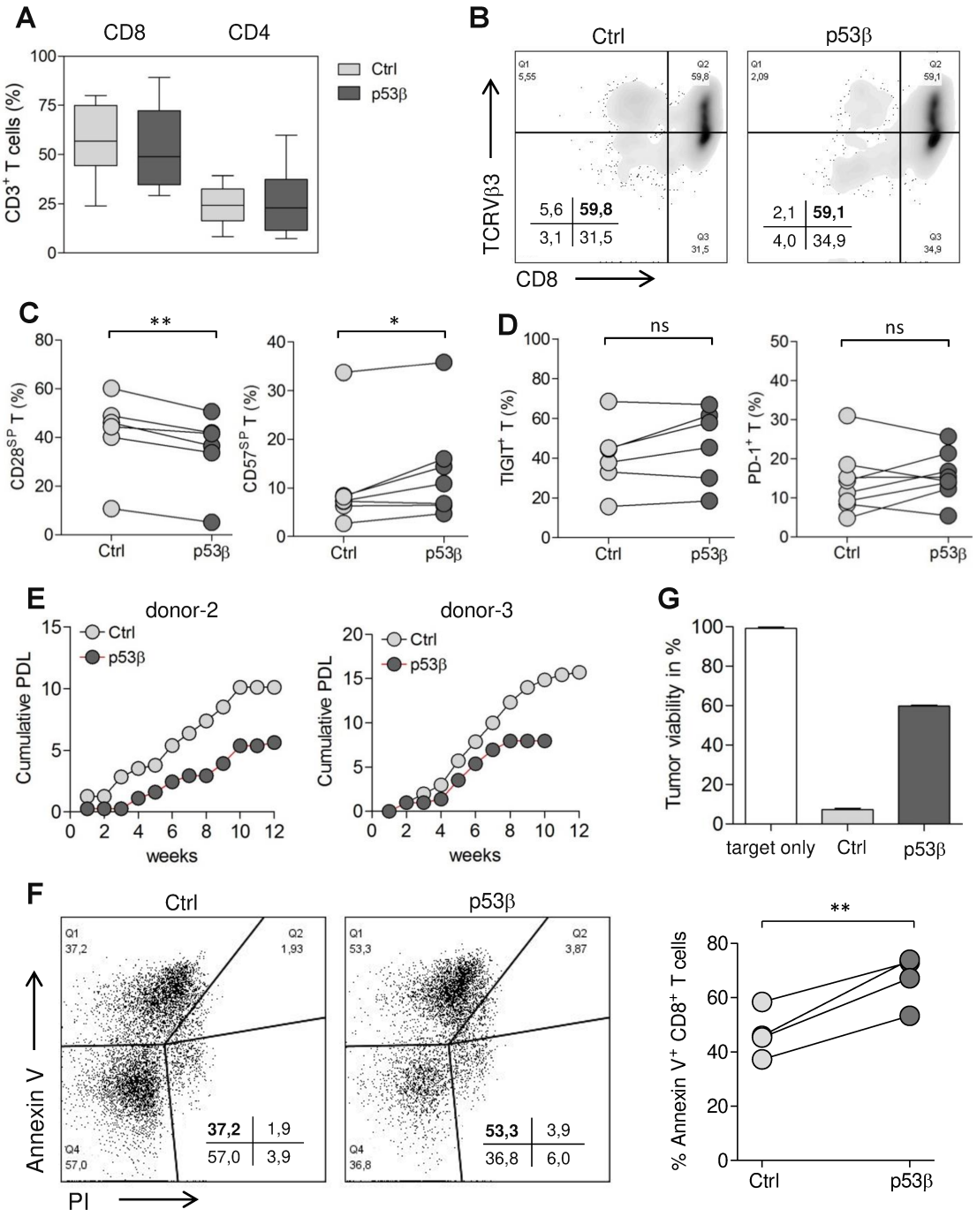


**Figure S3.** Characterization of p53β-driven senescence in engineered human CD8⁺ T cells. (A) Percentage of CD8⁺ and CD4⁺ T cells for paired samples of p53β-modified or control T cells from healthy donors (n=9 biological replicates). (B) Representative flow plots for the cell surface expression of the transduced scTCR in CD8⁺ T cells, which was determined by flow

jitc-2020-001846.R2

cytometry using anti-TCRVβ3 mAb. (C) Flow cytometry plots depicting cell surface expression of CD28 and CD57 single positive (SP) for paired samples of p53β-modified or control $CD8^+$ T cells from different donors (n≥6). (D) Difference in TIGIT and PD-1 expression between control and p53β-transduced cells shown for each individual donor (n≥6). (E) Cumulative PDL of control and p53β-transduced $CD8^+$ T cells over time from two representative donors. (F) Representative flow plots of Annexin V and Propidium Iodide (PI) staining for control and p53β-transduced T cells, and the corresponding graphs depicting individual donors (n=4). (G) Long-term cytolytic activity of p53β-modified compared to control T cells as determined by Tumor Colony-Forming Assay (see Methods section). One representative experiment out of four biological replicates is shown. *P < 0.05, **P < 0.01, ns (not significant), by two-tailed Student's *t* test.

jitc-2020-001846.R2

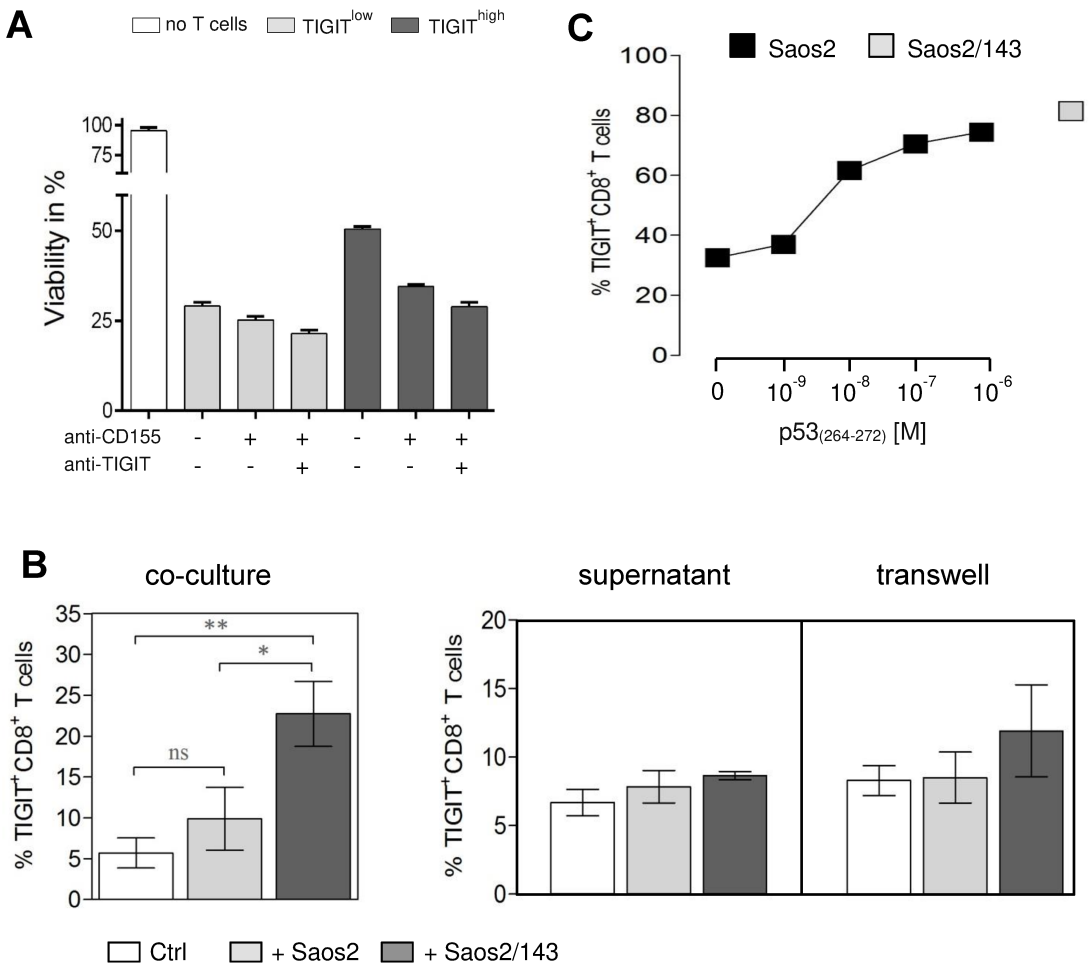


**Figure S4.** TIGIT expression in T cells is antigen-dependent and affects TCR-mediated cytolytic response. (A) Effect of CD155 and/or TIGIT blockade on the cytolytic activity of TIGIT$^{low}$ and TIGIT$^{high}$ TCR-effector T cells against Saos2/143 target tumors, as determined by tumor colony-forming based killing assays. (B) Flow cytometric data of TIGIT expression with or without incubation in cell-free supernatant collected from Saos2$^{p53null}$ or Saos2/143. TIGIT expression of T cells co-cultured with Saos2$^{p53null}$ or Saos2/143 under normal conditions or in transwell system. (C) TIGIT expression of CD8$^+$ T cells after co-culture with Saos2$^{p53null}$, which were pulsed with titrated concentrations of the target antigen ($p53_{264-272}$ peptide). n ≥ 3 biological replicates. Error bars indicate standard error of mean (SEM). *$P < 0.05$, **$P < 0.01$, ns (not significant), by two-tailed Student's *t* test.

jitc-2020-001846.R2

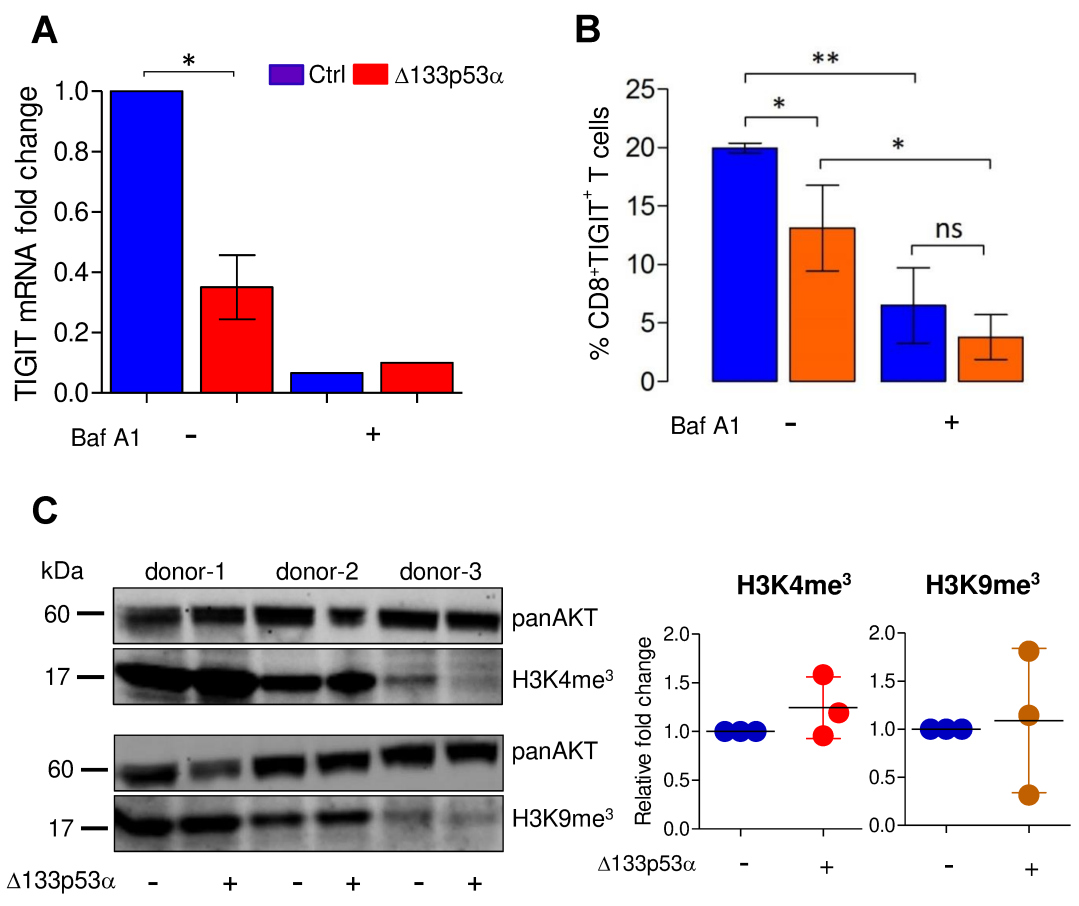


**Figure S5.** Δ133p53α role in the transcriptional regulation of TIGIT expression. (A) Change in fold expression of TIGIT mRNA in engineered human CD8⁺ T cells (1-3 weeks post transduction). T cells were treated with bafilomycin A1 for 24h and assessed by qRT-PCR for TIGIT transcripts. Error bars indicate standard error of mean (SEM) (n=3 biological replicates). One representative experiment is depicted for Baf A1 treatment. (B) Flow cytometric data showing the corresponding percentage of $CD8^+TIGIT^+$ T cells. Error bars indicate standard error of mean (SEM) (n=3 biological replicates). (C) Protein expression analysis of the histone marks H3K4me3 and H3K9me3 in engineered $CD8^+$ T cells from three different healthy donors (western blots, left panel) and the relative fold change in expression compared to control-T cells (histogram plots, right panel). $*P < 0.05$, $**P < 0.01$, ns (not significant), by two-tailed Student's *t* test.

jitc-2020-001846.R2

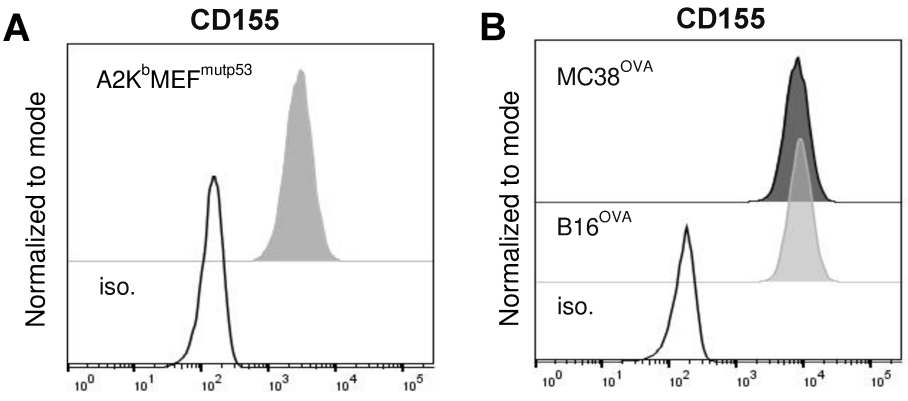


**Figure S6.** Expression levels of CD155 for A2K$^{b}$MEF$^{mutp53}$ (A) MC38$^{OVA}$ and B16$^{OVA}$ (B) were analyzed by flow cytometry.

jitc-2020-001846.R2

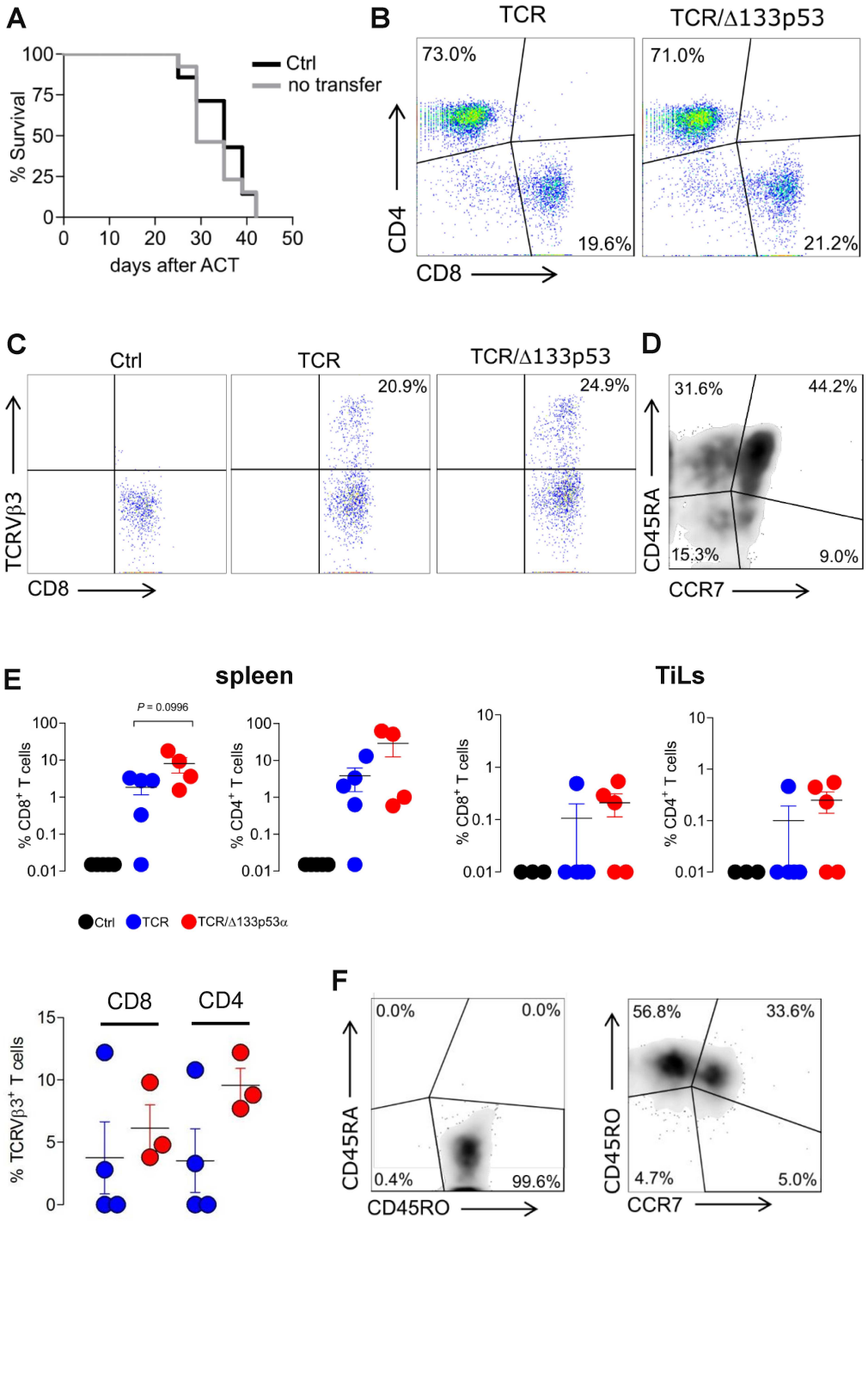

jitc-2020-001846.R2

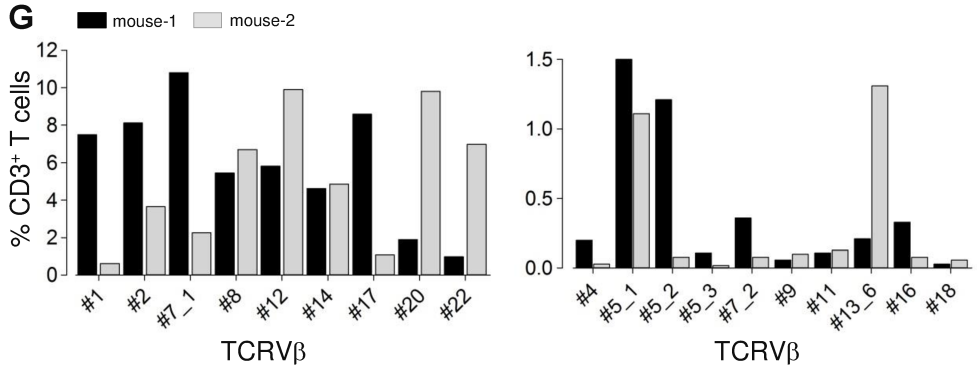


**Figure S7.** Phenotype and persistence of TCR/Δ133p53α-engineered T cells in vivo. (A) Survival curves for mice treated with mock-control modified T cells (Ctrl, n=13) or no transfer T cells (PBS only, n=7). Representative flow plots show comparable starting CD8/CD4 ratio (B) and TCRVβ3 expression (C) in Δ133p53α- and control-T cells at the time of infusion in mice. (D) Phenotype of engineered T cells prior adoptive transfer, determined by the expression of CD45RA and CCR7. (E) Frequency of tissue-infiltrating infused T cells as percent of CD8+ or CD4+ T cells per spleen or tumor (TiLs) in mice at day 40-60 (endpoint) after transfer. Data represent mean numbers +/- SEM from 4-5 mice in each group. The frequency of spleen-infiltrating TCR-specific CD8+ and CD4+ T cells is shown as percent of TCRVβ3+ T cells per tissue. (F) Phenotype of infused T cells in vivo, characterized by the expression of CD45RA, CD45RO and CCR7. (G) Analysis of the TCR Vβ repertoire of TCR-engineered T cells in vivo by flow cytometry with an antibody panel directed against 19 individual TCR/Vβ chains. Histograms depicting the frequency of high (left) and rare (right) T cell clones from isolated spleens of two representative mice.

jitc-2020-001846.R2

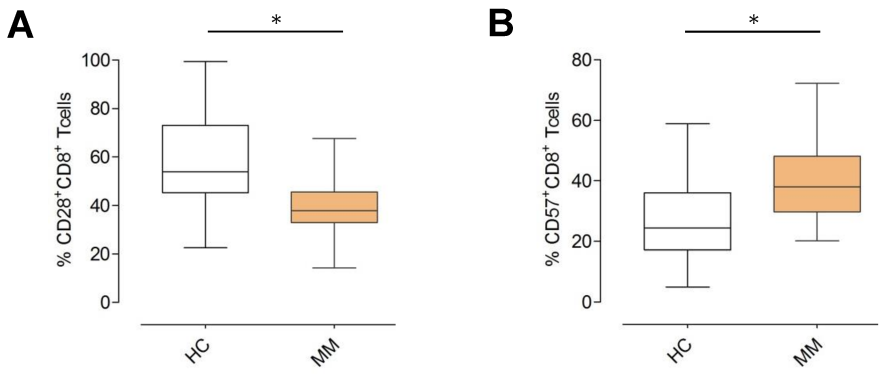


**Figure S8.** CD28 vs. CD57 expression profile in CD8⁺ T cells from multiple myeloma patients. (A) Box plots demonstrating the higher frequency of total CD28⁺CD8⁺ T cells in the peripheral blood from healthy controls (HC) compared to MM patients, as measured by flow cytometry (*P* = 0.0127). (B) Box plots showing the reduced frequency of total CD57⁺CD8⁺ T cells in HC compared to MM patients (*P* = 0.0166). HC (n = 15), MM (n = 10). *P* values determined by two-tailed Student's *t* test.

jitc-2020-001846.R2

1 **Table S1. Antibodies for flow cytometry**

| antibodies | clone | source |
|---|---|---|
| anti-human CD3, APC | UCHT1 | BD Biosciences |
| anti-human CD3, APC-R700 | UCHT1 | BD Biosciences |
| anti-human CD4, FITC | RPA-T4 | BD Biosciences |
| anti-human CD45, APC-H7 | 2D1 | BD Biosciences |
| anti-human CD8α, APC | RPA-T8 | BD Biosciences |
| anti-human CD8α, FITC | HIT8a | BD Biosciences |
| anti-human CD27, PE | M-T271 | BD Biosciences |
| anti-human CD27, APC | REA499 | Miltenyi Biotec |
| anti-human CD28, FITC | CD28.2 | BD Biosciences |
| anti-human CD28, PE | CD28.2 | BD Biosciences |
| anti-human CD57, APC | NK-1 | BD Biosciences |
| anti-human CD57, BV421 | NK-1 | BD Biosciences |
| anti-human CD62L, PC-5 | DREG56 | Immunotec |
| anti-human CCR7, FITC | 150503 | R&D Systems |
| anti-human PD-L1, APC | MIH1 | BD Biosciences |
| anti-human PD-1, APC | J43 | ThermoFischer Scientific |
| anti-human PD-1, FITC | MIH4 | BD Biosciences |
| anti-human PD-1, BV421 | EH1.21 | BD Biosciences |
| anti-human CD160, PE | BY55 | BD Biosciences |
| anti-human TIGIT, APC | REA1004 | Miltenyi Biotec |
| anti-human TIGIT, PE-Cy7 | A15153G | BioLegend |
| anti-human TIGIT, PE | MBSA43 | Invitrogen |
| anti-human CD155, APC | 300907 | R&D Systems |
| anti-human CD155, PE | SKII.4 | BD Biosciences |
| anti-human CD107a, PE-Cy5 | H4A3 | BD Biosciences |
| anti-human CD45RA, PE | HI100 | BD Biosciences |
| anti-murine TCRVβ3, PE | KJ25 | BD Biosciences |
| anti-human CD155 (neutralizing) | SKII.4 | BioLegend |
| anti-human TIGIT (neutralizing) | MBSA43 | eBioscience |
| anti-HLA-A2.1, PE | BB7.2 | BD Biosciences |
| Anti-human GLUT1-Alexa Fluor® 647 | 202915 | BD Biosciences |

jitc-2020-001846.R2

| | | |
|---|---|---|
| anti-murine TIGIT, BV421 | 1G9 | BD Biosciences |
| anti-murine TIGIT, PE | REA536 | Miltenyi Biotec |
| anti-murine PD-1, APC | J43 | Invitrogen |
| anti-murine CD155, PE | 3F1 | BD Biosciences |
| anti-murine PD-L1, PE/Cy7 | 10F.9G2 | BioLegend |

jitc-2020-001846.R2

**Table S2. Primers for qRT-PCR**

| Target | Forward | Reverse |
|---|---|---|
| TIGIT | TGCCAGGTTCCAGATTCCA | ACGATGACTGCTGTGCAGATG |
| GAPDH | GTTTACATGTTCCAATATGATTCCAC | TCATATTTGGCAGGTTTTTCTAGAC |